

Analysis of LBT LINC-NIRVANA simulated images of galaxies and young stellar objects

Paolo Ciliegi^a, Andrea La Camera^b, Gabriele Desiderá^b, Simone Antonucci^c, Carmelo Arcidiacono^d, Matteo Lombini^a, Emiliano Diolaiti^a, Enrica Bellocchi^a, Filippo Mannucci^e, Mario Bertero^b, Patrizia Boccacci^b, Dario Lorenzetti^c, Brunella Nisini^c

^aINAF - Osservatorio Astronomico Bologna, Via Ranzani 1, 40127, Bologna, Italy;

^b DISI, Genova University, Via Dodecaneso 35, 16146, Genova, Italy

^cINAF - Osservatorio Astronomico di Roma, Via di Frascati 33, 00040, Monte Porzio Catone, Italy;

^dINAF - Osservatorio Astronomico di Padova, Vicolo dell'Osservatorio 5, 35122, Padova, Italy;

^eINAF - Osservatorio Astronomico Arcetri, L.go E. Fermi 5, 50125, Firenze Italy

ABSTRACT

LINC-NIRVANA (LN) is a Fizeau interferometer that will provide for the first time coherent images in the near-IR combining the beams from the two Large Binocular Telescope (LBT) arms, by adopting a Multi-Conjugate Adaptive Optics system (MCAO) that allows for atmospheric turbulence compensation. We applied a software for the simulation and the reconstruction of LN images (AIRY-LN, see Desiderá et al.¹ this Conference) in two specific scientific cases: a relatively distant galaxy at redshift about 1 and a collimated jet from a Young Stellar Object (YSO). These two cases have been chosen to test the capability of LN in the observations of faint and small (1-2 arcsec) extragalactic objects and objects with diffuse emission and high dynamical range, respectively. A total of six images at different hour angles have been obtained for both cases. Using these simulated images, we obtained the final reconstructed images using the software package AIRY-LN. These images have been analyzed with the standard data reduction software (IRAF and IDL). Our analysis show that the reconstruction algorithm is fundamental to obtain a good reproduction of the original flux and morphology while the optimal number of iterations strongly depends on the scientific goal.

Keywords: Image simulations, galaxies, young stellar objects

1. INTRODUCTION

The Large Binocular Telescope (LBT, Hill and Salinari²) currently operating on Mount Graham in Arizona with its two 8.4 m mirrors, is an ambitious and innovative undertaking to construct one of the world's largest optical and infrared telescopes. LINC-NIRVANA (LN) (Herbst et al.³, Bizenberger et al.⁴) is a near-infrared image-plane beam combiner with Multi-Conjugate Adaptive Optics system (MCAO), allowing for atmospheric turbulence compensation. The MCAO systems aboard each LBT arm use the light of wavelength $0.6 < \lambda < 1.0 \mu\text{m}$ for wavefront sensing, while the science observations are performed in the wavelength range $1.0 < \lambda < 2.4 \mu\text{m}$, i.e. the range including the J, H and K bands. The fringe tracking, i.e. the measurement of the optical path difference between the two LBT arms, is performed in the near infrared as well.

The performance of the LN interferometer is expected to be very close to the diffraction limit. Due to the binocular nature of the instrument, the Point Spread Function (PSF) may be described as the diffraction limited pattern of an 8.4 m telescope crossed by the fringes due to the interference between the two apertures, characterized by a maximum baseline of approximately 22.8 m. For this reason, the raw images obtained with LN will have an anisotropic angular resolution: typical of an 8 meter class telescope in one axis, approximately 3 times better in the orthogonal axis. The maximum resolution, in the direction of the maximum baseline, ranges from approximately 0.01 arcsec in the J band to 0.02 arcsec in the K band. If exposures are taken at different hour angles in order to obtain a better uv-coverage, an aperture synthesis image reconstruction procedure can provide reconstructed images with the full angular resolution of a 22.8 m single-dish telescope.

The scientific camera is a 2048×2048 infrared array inside a cryostat. The camera optics have a fixed focal length, corresponding to a plate scale of 0.005 arcsec/pixel, which allows to sample the PSF at the Nyquist limit in all conditions. The science field of view is therefore 10×10 arcsec. The technical field of view is larger. The fringe tracker has in fact a field of view of 1×1.5 arcmin.

Here we will present the simulation and the reconstruction of LN images in two specific science cases: a relatively distant galaxy at redshift ~ 1 and a Young Stellar Object (YSO) with its collimated jet. A detailed analysis of these simulations will give us fundamental information on the capability of LN to observe faint and small (~ 1 -2 arcsec) extragalactic objects, or, alternatively, the high dynamic range fields where diffuse emission arises from the vicinity of strong point sources.

1.1 Scientific aims of the observations

1.1.1 Galaxies at $z \sim 1$

The observation of extragalactic sources with the very high resolution of LN will give us fundamental information in many different fields. Imaging of $z \sim 1$ -2 galaxies, Active Galactic Nuclei, galaxies' morphology and interactions, star-forming regions in galaxies are only a few of the many different fields that will receive new input from observations with LN.

Here we will concentrate on the imaging of $z \sim 1$ galaxies and in particular on the capability of LN to study the surface brightness profile with a resolution and sensitivity never reached before by ground-based observations. Parametric fits to the surface brightness profile can be used to classify the central structure and to search for possible supermassive black holes and Active Galactic Nuclei. The well defined correlation between the black hole mass and bulge luminosity will allow to evaluate the masses of the active central engines.

1.1.2 Jets from Young Stellar Objects

The goal of the LN observations related to this scientific topic is to investigate the base of IR jets from young stellar objects (YSOs) through imaging in narrow-band filters centered on two bright tracers, namely the H_2 at $2.12 \mu\text{m}$ and [FeII] at $1.64 \mu\text{m}$. The understanding of the ejection process in young stars is fundamental being this process intimately related to the protostar accretion and to the need to remove the excess of angular momentum (e.g. Königl & Pudritz⁵). Different mechanisms have been proposed for the jet formation and propagation (Garcia et al.⁶, Shang et al.⁷), which however need high spatial resolution observations to be tested. Indeed, protostellar jets are accelerated and collimated in regions within a few tens of AU (i.e. 0.1-0.5 arcsec in the nearby star forming regions). The jet is expected to be collimated already very close to the driving source, with widths below 0.5 arcsec in nearby YSOs. The degree of collimation close to the source is an important parameter to discriminate the different models. Another important observational constraint comes from the morphology of the jet at sub-arcsec resolution: it should be tested if the jet is uniform close to the protostar or can be resolved in emission knots, which can testify the occurrence of different accretion events on timescales of a few years. In this respect, also an accurate measure of each knot centroid, done on images taken at different times, should be performed in order to have proper motion measurements.

This analysis should be performed using both atomic ([Fe II]) and molecular (H_2) transitions, in order to probe both the more excited gas expected to trace the inner jet section, and the colder molecular gas ejected from the external layer of the jet (e.g. Nisini et al.⁸). This simulation, in particular, has been performed assuming an observation with a narrow band filter centered on the H_2 line at $2.12 \mu\text{m}$.

2. DATA SIMULATION

2.1 Raw input data : Description and Preparation

2.1.1 Galaxy at redshift $z \sim 1$

To test the very high angular resolution of LN in the observations of relatively distant galaxies we have simulated an observation of a galaxy at $z \sim 1$. To do this, we have generated a synthetic image of a $z \sim 1$ galaxy starting from a real high resolution image of a galaxy at $z \sim 0.1$ obtained with the Hubble Space Telescope (HST). In this way we were able to study all the relevant parameters on the initial "real" low redshift image and then repeat the analysis on the same galaxy "moved" to $z \sim 1.0$ and "observed" with LN.

In order to simulate the expected emission from a galaxy at redshift about 1, the galaxy at $z\sim 0.1$ in the original image with a dimension of ~ 7 arcsec has been scaled down to a dimension of ~ 1 arcsec according to the canonical angular size-distance relationship, while the pixel scale of the image was changed to 5 mas/pixel to match the LN resolution. The galaxy has been rebinned with a factor of about 1.4, moving the dimension of the galaxy from the original 140 pixels to 200 pixels. Finally a magnitude of $K_s=18.0$ has been assumed for the scaled galaxy at $z\sim 1$, while an average K-band sky brightness of $13.5 \text{ mag/arcsec}^2$ has been assumed as background emission. The simulated images at $z\sim 1$ is reported in Fig. 1 (left side).

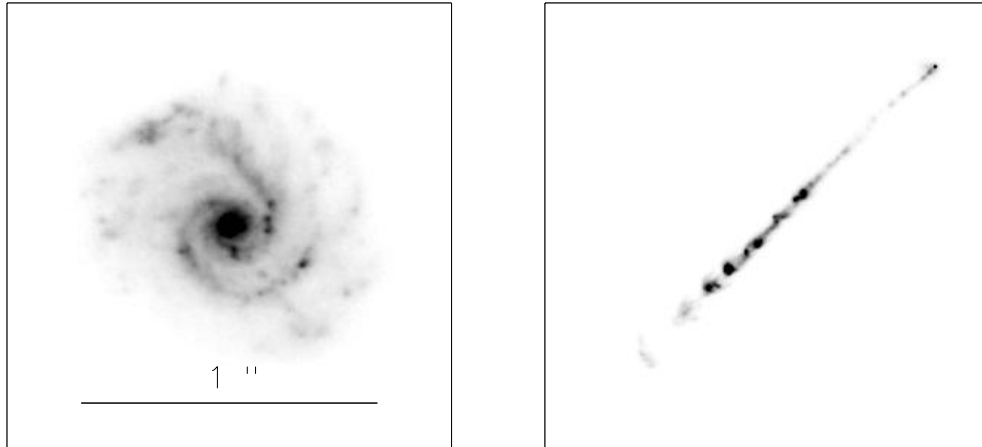


Figure 1. *Left:* Simulated galaxy at $z\sim 1$ obtained scaling down the galaxy at $z\sim 0.1$ to a dimension of ~ 1 arcsec and changing the pixel scale from 50 to 5 mas/pixel. The dimension of this image is 300×300 pixels corresponding to 1.5×1.5 arcsec (pixel scale 5 mas/pixel). *Right:* The synthetic image of the Young Stellar Object HH34 used for the simulation. The pixel scale of this image has been set to 5 mas/pixel.

2.1.2 The Jets of Young Stellar Objects

To construct the synthetic image for the simulation, we have considered an optical image taken with HST of the HH34 jet (Reipurth et al.⁹). The image has been taken with the WFPC2 in a filter centered on the [SII]6730Å line, has a pixel size of 70 mas and does not contain the emission from the driving star, because the latter is heavily embedded and thus is not optically visible.

Starting from this image, we have performed the following steps in order to obtain a synthetic image simulating the expected emission in a narrow band filter centered at $2.1218\mu\text{m}$ and having a FWHM of $0.02\mu\text{m}$: 1) the pixel scale of the image was changed to the 5mas/pixel of LN and the integrated magnitude of the jet normalized to 13 mag, in order to roughly reproduce the H_2 $2.12\mu\text{m}$ brightness of $\sim 10^{-14} \text{ erg s}^{-1} \text{ cm}^{-2} \text{ arcsec}^{-2}$ typically observed in protostellar jets; 2) a point source having a K magnitude of 13 mag was added to the image at the position where the HH34 infrared driving source is located; 3) the average K -band sky brightness of $13.5 \text{ mag/arcsec}^2$ measured on Mauna Kea has been assumed as background emission.

The final image is shown in Fig. 1 right side. We point out how in this case, as in most cases dealing with observations of star-forming regions, there is not any other bright star in the LN field of view available to measure, in the acquired images, the PSF to be used in the image reconstruction procedure. The PSF should therefore be either assumed or measured directly on the jet driving source, with the limitations given by the contamination from the jet diffuse emission.

2.2 Description of Simulated Observing Scheme

For both cases (galaxy and YSO) we assumed that a total of six images at different equispaced hour angles have been obtained. In particular we assumed that the galaxy will be observed with parallactic angles of 0,30,60,90,120

and 150 degrees while the YSO with parallactic angles of -90 , -45 , -15 , 15 , 45 and 90 degrees. Each single image has been obtained assuming an integration time of 30 minutes, for a total integration time of 3 hours. The background has been assumed equal to $13.5 \text{ mag/arcsec}^2$ while dedicated sky observation have not been simulated.

2.3 Simulation of Observing Condition (PSF)

The PSF are generated through the software LOST (Arcidiacono et al.¹⁰). LOST is a numerical tool implemented for the simulation of Multi-conjugate Adaptive Optics (MCAO) systems using the Layer Oriented approach. In particular this code is the only one able to simulate the Multiple Field of View (MFoV) MCAO technique (Ragazzoni et al.¹¹) as it will be implemented in the LN instrument. Moreover it is able to combine the two adaptive optics arms providing an adaptive optics corrected LBT-interferometric PSF.

This tool has been completed by adding some ad-hoc routines used to compute rotation angle and airmass, and to include the effect of the polychromatism on the PSF. In fact LOST computed PSFs are purely monochromatic: in order to simulate the effect of different wavelengths we applied the reasonable approximation of piling up on a single array different copies of the same monochromatic PSF, scaled in angular size in accordance with the wavelength.

2.4 Exposure Construction and Convolution

The construction of the single exposure has been performed using modules of the software package AIRY (Astronomical Image Restoration in interferometrY), version 4.0. A description of the structure of the package, which is modular, based on IDL and designed to be used together with the CAOS (Code for Adaptive Optics Systems) Application Builder (see Fini et al.¹²), is given in Correira et al.¹³

In the following we indicate the modules of AIRY that must be used in the different steps of a generic simulation/reconstruction project.

2.4.1 Image simulation

A simulation project consists of the following steps.

- The user must provide the hour angles of the observations and the object, including additional parameters and precisely: the observation band, the magnitude of the object, the pixel size and the total dimension of the image (in pixels). In this way the FoV, in arcsec, is given. Then it is possible to change the size of the object (in arcsec) within the FoV.
- The user must provide a stack of PSFs, one for each hour angle, all with vertical fringes.
- The module RTI (RoTate Image) is used to generate a stack of rotated objects corresponding to the rotation angles given in step 1 (this step can generate artifacts, in particular in the case of point objects/stars). In general a rotated object is immersed in a broader array and surrounded by zeroes.
- The stacks of objects and PSFs are the inputs of the module CNV (CoNVolution); additional parameters that must be provided are: telescope aperture, integration times for the different angles, total efficiency. The output is a stack of noise-free images.
- Use the module ADN (ADd Noise) to corrupt the images with background, photon noise and read out noise (RON); the user must provide the magnitude of the background and the σ of the RON. It is also possible to add dark current and saturation. The output is a stack of simulated LINC-NIRVANA images corresponding to the given object.

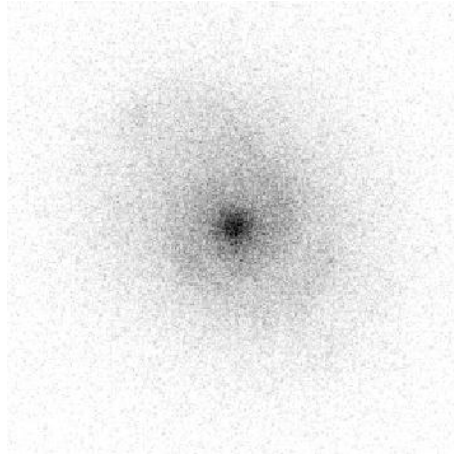


Figure 2. The image obtained by co-adding the six single exposure images.

2.4.2 Galaxy case

Six different images at 6 different parallactic angles (0,30,60,90,120 and 150 degrees) have been obtained following all the steps described above. As input object, we used the image described in sections 2.1 and 2.2 while the PSFs used at each hour angle have been obtained using the software LOST (see section 2.3).

In Fig. 2 we show the image obtained by derotating each of the six images to the same parallactic angle and then co-adding all of them.

2.4.3 YSO case

As for the case of the galaxy at $z \sim 1$, also for the YSO case we obtained 6 different images following all the steps described in Section 2.4. The images have been obtained with parallactic angles of -90 , -45 , -15 , 15 , 45 and 90 degrees, using as input the object described in section 2.1.2 (Fig. 1), 6 PSFs calculated with LOST and assuming an integration time of 30 minutes for each image.

2.5 Image Deconvolution and Reconstruction

The image reconstruction has been performed using modules of the software package AIRY-LN, a numerical tool for deconvolution of images from LINC-NIRVANA. A detailed description of AIRY-LN is reported in another paper presented in this Conference (Desiderá et al.¹). The basic algorithm used is described in Bertero & Boccacci¹⁴ and denoted OSEM (Ordered Subset Expectation Maximization); it was introduced in tomography by Hudson & Larkin.¹⁵ This algorithm is essentially an accelerated version of the Richardson-Lucy method (RLM) and has been subsequently modified to compensate for both object rotation and boundary effects (La Camera et al.¹⁶).

A reconstruction project consists of the following steps.

- Provide the stack of images and the corresponding hour angles. It is also possible to provide a stack of corresponding PSFs (with vertical fringes) to be used for deconvolution in place of the stack of PSFs of step 3 below. If the PSFs coincide with those used for convolution, the deconvolution based on these PSFs is what we call *inverse crime*.
- Use the module LDR (Ln DeRotation) for derotating the images. In the case of inverse crime reconstructions a more accurate derotation of the PSFs is performed in Fourier space. The PSFs are expanded by zero padding, then the following sequence of operations is performed: shift, FFT, shift, derotation with IDL function *rot*, shift, inverse FFT, shift.
- Use the module LPX (Ln Psf eXtraction) for extracting and extrapolating the PSF from one or more stars in the FoV of the derotated images. The result is a stack of derotated PSFs.

- Use the module LMD (Ln Multiple Deconvolution) for reconstructing the object. The input consists of two stacks, one of images and one of PSFs; the output is the reconstructed object. The number of iterations is an additional parameter that must be provided by the user.

2.5.1 Image reconstruction results

Using the single exposure and the procedure described above, we obtained the final reconstructed image for each scientific case. To keep the simulation as simple as possible, in both cases the PSF for the deconvolution process has been not extracted from the images: we used the same PSF used in the convolution (*inverse crime*). In this way our simulation provides the best reconstructed object obtainable from the data.

As described in section 2.5 the final output of the reconstruction process is the final reconstructed image. This image is obtained after a given number of iterations, number that must be specified by the user. However, since one of the main goals of our work is to test the performance of the method, for each scientific case we produce several reconstructed images obtained with an increasing number of iterations.

At each iteration we compute the relative r.m.s. error defined by

$$\rho^{(k)} = \frac{\|\mathbf{f}^{(k)} - \mathbf{f}\|_2}{\|\mathbf{f}\|_2}$$

where $\mathbf{f}^{(k)}$ is the result of the k -th iteration, \mathbf{f} is the original object and

$$\|\mathbf{f}^{(k)} - \mathbf{f}\|_2^2 = \sum_n |f^{(k)}(n) - f(n)|^2$$

with a similar definition for $\|\mathbf{f}\|_2$.

As a function of k , $\rho^{(k)}$ has a minimum corresponding to an “optimum” number of iterations. For each experiment we give this value as a percentage error of the reconstruction of the object.

With several reconstructed images available, we will be able to selected the best compromise between a low number of iterations and a high quality of the reconstructed image; however the definition of the quality of a reconstructed image strongly depends on the scientific goal of each project and must be judged by an accurate scientific analysis, not only on the basis of the relative r.m.s. error.

2.5.2 Reconstructed images

In Fig. 3 we show two reconstructed images for the galaxy obtained with 300 and 1000 iterations.

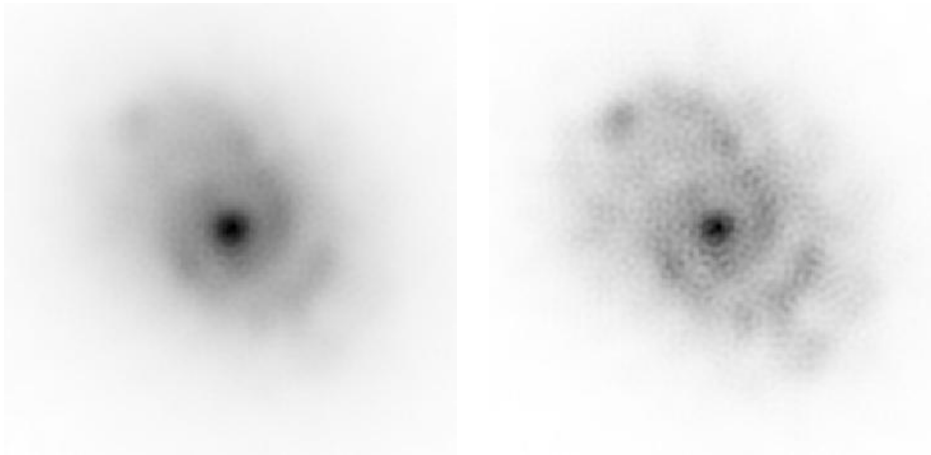


Figure 3. The reconstructed images of the galaxy at $z \sim 1$ obtained with 300 (left) and 1000 iterations (right)

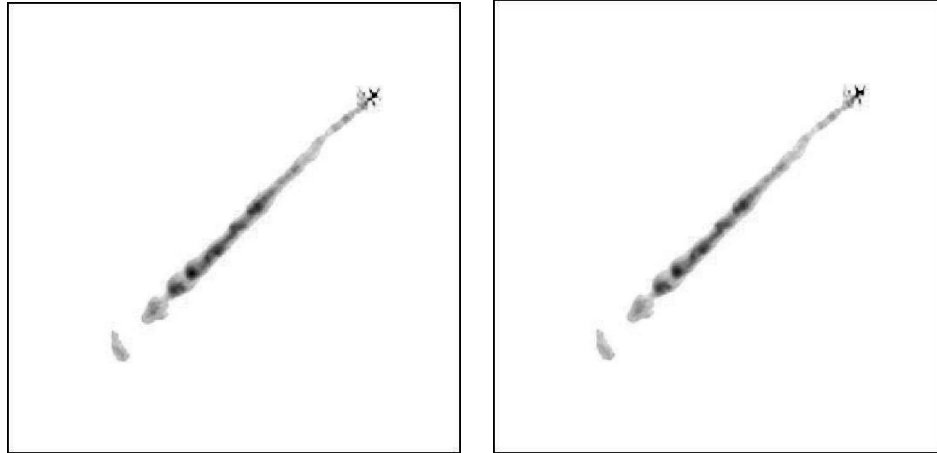


Figure 4. Reconstructed image for the jet in the YSO using the standard reconstruction algorithm (left) and the modified reconstruction algorithm with regularization (right). The two images have been obtained with 750 iterations.

In the case of the jet of the YSO HH34, we performed two different reconstructions: a standard reconstruction algorithm with the 6 single exposure images and a modified reconstruction using an algorithm with regularization (Anconelli et al.¹⁷). The regularization method has been developed for the reconstruction of images with high dynamic range

In Fig. 4 we show two reconstructed images for the two cases listed above. The two images have been obtained with 750 iterations.

3. DATA ANALYSIS

3.1 Analysis of the reconstructed image of a $z \sim 1$ galaxy

We have analysed the non-reconstructed image obtained by co-adding the six images at different parallactic angle plus the reconstructed images of the galaxy obtained with 300, 500, 750 and 1000 iterations in order to make a comparison with the original image.

Total Flux. As a first step we measured the total flux of the galaxy by means of concentric aperture photometry with the *aper* function in the *Astrolib* IDL library. We used several aperture radii: from a very small value to a radius that includes the whole galaxy. For the original image and for the two reconstructed images no sky background subtraction has been done : the original image is that described in Section 3 while in the reconstructed images the background is removed by the reconstruction algorithm. In the non reconstructed image the background has been removed in two different ways: using the theoretical background of $13.5 \text{ mag/arcsec}^2$ (corresponding to 7541.3 counts/pixels), or using a background estimated in the outer regions of the image. In Fig. 5 (left side) we show the total flux of the galaxy as a function of the aperture radius for the original image (solid line), for the reconstructed images obtained with 300 (dot dashed line) and 1000 (dashed line) iterations and for the non reconstructed image with different background subtraction (dot dot dot dashed for the theoretical background, dotted lines for a background estimated in two different regions of the image).

As shown in figure, the galaxy flux measured in the reconstructed images is in good agreement with the original flux. The reconstructed flux is $\sim 100\%$ of the original flux in the central region up to 70 pixels (0.35 arcsec) and becomes $\sim 98\%$ (with 300 iterations) and $\sim 99\%$ (with 1000 iterations) when we consider the whole galaxy.

The situation is different when we consider the non-reconstructed image. In this case we have only $\sim 50\%$ of the original flux in the central region (70 pixel radius) and a fraction of the flux between 70 - 80 % (depending on the background subtraction) when we consider the whole galaxy. A large fraction of the galaxy flux is spread in

the outer regions of the image, making the photometric accuracy very poor and strongly dependent on a correct sky subtraction.

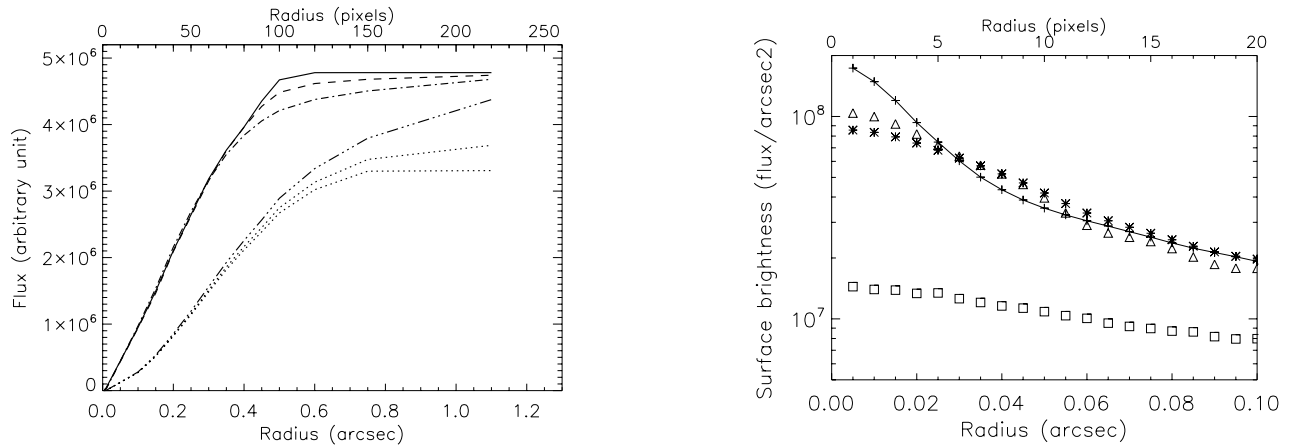


Figure 5. *Left:* The total flux of the galaxy as a function of the aperture radii for the original image (solid line), for the reconstructed images obtained with 300 (dot dashed line) and 1000 (dashed line) iterations and for the non reconstructed image with different background subtractions (dot dot dot dashed for the theoretical background, dotted lines for a background estimated from the image). *Right:* The galaxy surface brightness profiles for the original image (crosses plus solid line), for the reconstructed images with 300 (stars) and 1000 (open triangles) iterations, and for the non reconstructed image with the theoretical noise subtracted (open squares) in the central 0.1 arcsec.

Radial Surface Brightness Profile.

We analysed the radial surface brightness profile of the galaxy considering two different regions: a circle of radius 70 pixels (0.35 arcsec) where the reconstructed flux is ~100% of the original one (see above) and a circle of radius 100 pixels (0.5 arcsec) that includes the whole galaxy.

In order to examine whether the light profile of the reconstructed images is similar to that of the original galaxy or not, we applied a one-component Sérsic profile fitting to all the images considered. For the profile fitting process we used the GALFIT software (Peng et al.¹⁸). The Sérsic profile is given by

$$I(r) = I_e \exp(-k_n((r/r_e)^{1/n} - 1))$$

with the surface brightness $I(r)$ at a radial distance r , and a surface brightness I_e at r_e , the effective radius or the half-light radius. The index n determines the shape of the profile; a profile with large n shows a more concentrated core and a more extended wing, while a profile with a smaller n shows a flatter core with a sharper cutoff. Disk-like galaxies (Sb/Sc/Irr) have profiles with $n=1$ while the profile of spheroid-dominated galaxies (E/S0/Sa) has $n=4$.

For both the circles used (70 and 100 pixels), the surface brightness profiles are very well reproduced in all the reconstructed images considered, although by increasing the number of iterations we obtain a better representation: The half-light radius r_e and the Sérsic index n converge towards the original values. Finally, the fit procedure failed for the image profile of the non reconstructed image.

In Fig. 5 (right side) we report the surface brightness profiles for the original image (crosses plus solid line), for the reconstructed images with 300 (stars) and 1000 (open triangles) iterations, and for the non reconstructed image with the theoretical noise subtracted (open squares).

In conclusion, for an accurate analysis of the surface brightness profile probably a high number of iterations are needed, while for a simple discrimination between disk-like profile and spheroid-like profile galaxies an iteration number of 300-400 appears to be sufficient. However, more specific simulations on this aspect with several (simulated ?) original images with different profile are needed to better investigate the capability of LN to distinguish between different classes of objects.

Conclusions and final remarks can be summarised as follows:

- **Photometry.** The reconstruction algorithm is fundamental to obtain a good photometry of the objects. In fact, while in the reconstructed images the flux recovered is more than 98% of the original one, in the non reconstructed images the flux recovered can be lower than 50%.
- **Iterations** The optimal number of iterations strongly depends on the scientific goal. For example, while a low number ($\sim 300-400$) of iterations could be enough for photometric studies or for a simple discrimination between one-component surface brightness profiles, a higher number of iterations could be required for detailed morphological studies or for accurate, multi-component profile fitting.

3.2 Analysis of the reconstructed image with a YSO

We have analysed the 2 sets of reconstructed images, the first obtained using the standard algorithm and the second with the version of the algorithm optimised to treat images with a high dynamic range. We will call these algorithms as LND and HDR, respectively.

Each set is composed of 5 reconstructed images, obtained with a different number of iterations (namely 150, 300, 450, 600 and 750).

All the images were rotated by 45 degrees before the analysis (using a bilinear interpolation and producing output frames of 340x340 pixels), so as to have the jet parallel to the y axis. Then we have analysed the images line by line, i.e. at different positions along the jet: this means that we get a series of spatial profiles of the jet (in a direction perpendicular to its axis). We have based the comparison between original and reconstructed images mostly on the properties of these profiles. Of each profile we have analysed the shape, the total flux and the width.

The main remarks from the various steps of such analysis are reported hereafter.

Images. We have performed a direct comparison between original and reconstructed images taking into account the pixel count differences (i.e. simply subtracting one image from the other). An indication of the global quality of the image reconstruction is then given by the quadratic sum of such differences. The images of the two sets do not substantially differ from each other; slightly smaller differences are obtained for the images with an intermediate number of iterations in both sets. The main problems in the reconstructed frames are related to the star region, where it is evident (also by a direct eye inspection) the presence of artifacts produced by the reconstruction process (see Fig. 6).

Total Flux. The star flux (in a circular aperture with a radius of 4 pixels) and the integrated jet flux measured in the reconstructed images amounts to $\sim 95\%$ and 92% (respectively) of the fluxes measured on the original image. Again, there are basically no differences among all the images of the LND or HDR sets.

Spatial Profile Shape. A direct analysis of the spatial profiles obtained in the region around the star clearly shows the problems due to the artifacts (see Fig. 7), which destroy the profile in the close surrounding of the exciting source. Profile shapes seem to be reproduced reasonably well up to a distance of ~ 20 pixels from the star; this means an angular distance of about 100 mas for the considered case.

Profile Flux and Width. The profile flux and width have been analyzed in function of the position along the jet (y-axis of the images), comparing the results on the original image to the ones obtained in both the reconstructed datasets (LND and HDR).

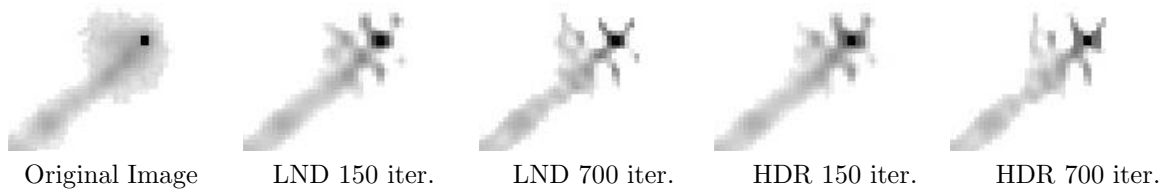


Figure 6. Comparison between the object image and the reconstructed images (with different iteration numbers) in the region around the star. Artifacts are clearly visible.

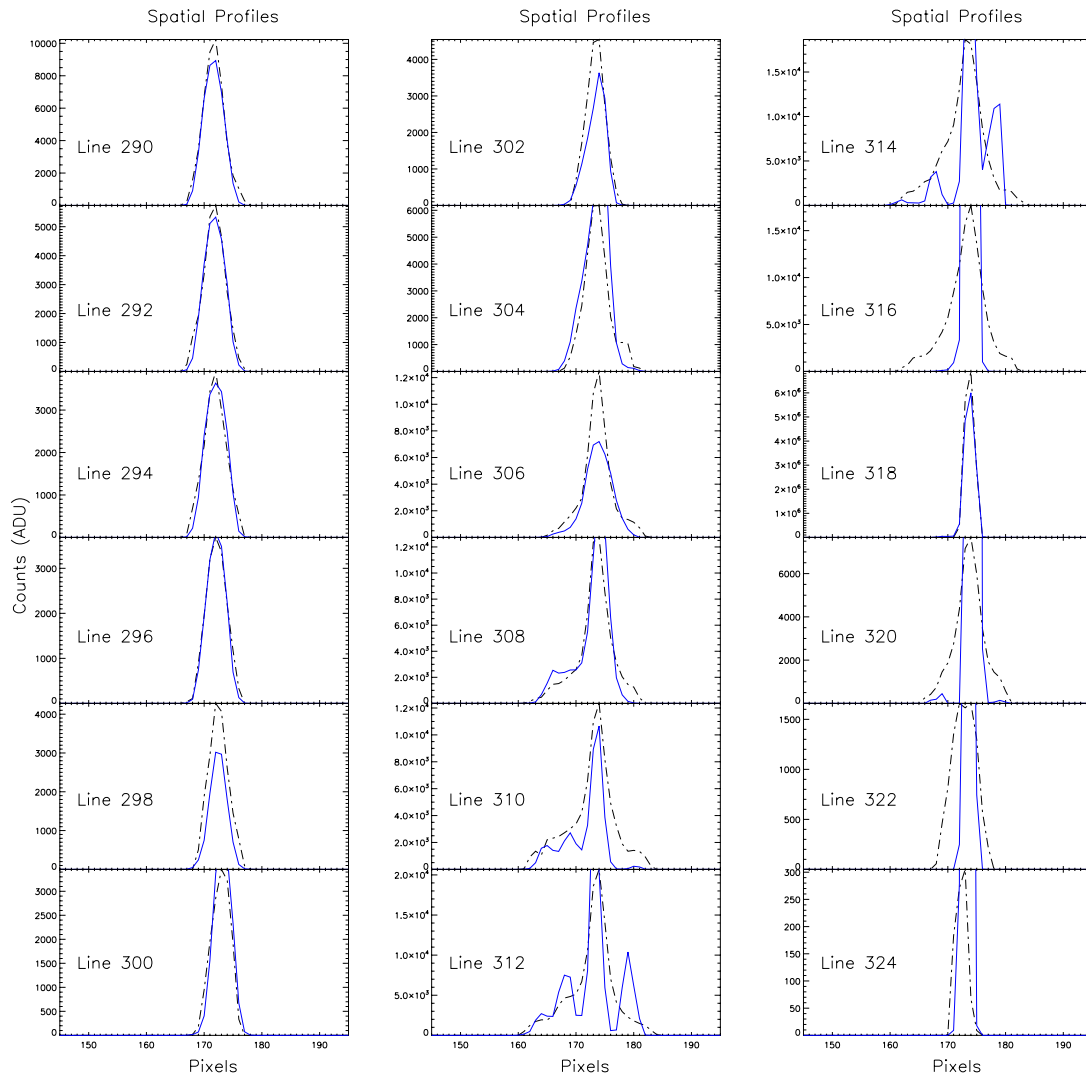


Figure 7. **LND images** - Series of spatial profiles of the object in the region around the star for the third (400 iterations) LND image (solid line). The dashed dotted line refers to the original image profile. The star centre is on line 318.

- **Flux.** The flux of the various spatial profiles is reproduced basically in the same way in each reconstructed image, independently of the number of iterations and algorithm used. The average error is less than 20%. In the region around the star the error increases rapidly, being above 30% at distances less than 20 pixels

from the star (i.e. ~ 100 mas), i.e. where the artifacts deform the profile shapes, as pointed out in the previous section. In this region there is no clear trend allowing us to identify the best reconstructed image.

- **Width.** For the width computation we cannot use a Gaussian FWHM, since the profile of the jet is in general not Gaussian. Thus, we have set an arbitrary count threshold and defined the width of the jet as the number of pixels lying between the first and the last pixel (along the considered line) that have a number of counts greater than the threshold (NOTE: the reconstructed images have no noise). The width is a key parameter, since it is directly related to the "diameter" measurement one should perform on the jet, with the aim of going as close as possible to the exciting source. In both the LND and HDR sets we note a trend: the width appears too large if we consider images with the lowest number of iterations (150). On the contrary, images obtained with a high iteration number (600 and 700) seem to be too narrow. The best results are found for images with 300-450 iterations. This is visible in both the jet and star regions. In the 300 and 450 iteration images the relative error remains less than 20% up to 3-4 pixels (~ 15 -20 mas) from the star; however, this result appears to be not reliable. Indeed, we have seen that the jet spatial profile shape and flux are heavily corrupted by the artifacts of the reconstruction process in a 20 pixel region around the star, so that a diameter measurement seems to be unfeasible inside this area.

Conclusions and final remarks can be summarised as follows:

- **LND and HDR sets.** In general, there is no significant difference between LND and HDR images, not only in the jet region, but also in the zone around the star where the high dynamic range optimisation should provide better results.
- **Iterations.** A maximum iteration number of 300-450 appears suitable to reconstruct the images.
- **Accuracy.** In the case analysed here (i.e. with the adopted star/jet brightness ratio of 1) the reconstruction allows us to reproduce the original jet image down to ~ 100 mas from the source with an error $< 20\%$ on flux and width. For comparison, the jet acceleration region we aim to study extends typically from 1 to 50 AU (i.e. from ~ 6 to ~ 300 mas at $D=150$ pc). We can therefore only marginally resolve this region in the near-by jets.

4. SUMMARY AND CONCLUSION

In this document we report the results of our work on the simulation and reconstruction of LN images in two specific science cases: a relatively distant galaxy at redshift ~ 1 and a Young Stellar Object (YSO) with its collimated jet. Starting from HST images we simulated the expected emission from a galaxy with a magnitude $K_s=18$ and from a YSO with an integrated magnitude of $K_s=13$. For both cases a K-band background emission of 13.5 mag/arcsec² has been assumed while the pixel scales of the simulated images has been set to 5 mas/pixel to match the LN resolution.

A total of six images at different equispaced hour angles have been obtained for both cases. Each single image has been obtained assuming an integration time of 30 minutes, for a total integration time of 3 hours. Using these simulated images, we obtained the final reconstructed images using the software package AIRY-LN. In order to test the performance of the method, for each scientific case we produce several reconstructed images obtained with an increasing number of iterations. Finally all the reconstructed images have been analyzed with the standard data reduction software (IRAF and IDL).

Our general conclusions can be summarised as follows:

- The reconstruction algorithm is fundamental to obtain a good reproduction of the original flux and morphology. For example, in the reconstructed images of the galaxy the flux recovered is more than 98% of the original one while in the non reconstructed images the flux recovered can be lower than 50%. For the YSO, the reconstruction algorithm allows us to reproduce the original flux and width with an error $< 20\%$.

- The optimal number of iterations strongly depends on the scientific goal. This is true for both the scientific cases analyzed. A low number (~ 300 -400) of iterations has been sufficient to reproduce the image of the YSO and for a simple discrimination between one-component surface brightness profiles of the galaxy. However, higher number of iterations are required for detailed morphological studies.

Our next steps will be the analysis of more realistic cases, with PSF extracted from the images, more realistic (and less numerous) parallactic angles, with fainter galaxies and with simulated images. In the YSO case, we also plan to simulate a different observational approach, namely to subtract an image of the source continuum from the image acquired with the filter centered on the line emission, in order to overcome the problem of the strong source continuum residuals in the reconstructed image.

REFERENCES

- [1] Desiderá, G., La Camera, A., Boccacci, P., Bertero, M. and Carbillet M., *AIRY-LN: an ad-hoc numerical tool for deconvolution of images from the LBT instrument LINC-NIRVANA*, *Proc. SPIE (this proceeding)* (2008)
- [2] Hill, J.,M. and Salinari, P. *The Large Binocular Telescope Project SPIE 4837, 15* (2003)
- [3] Herbst T.M., et al., *LINC-NIRVANA: A Fizeau Beam Combiner for the Large Binocular Telescope SPIE 4838, 456* (2003)
- [4] Bizenberger, P., Diolaiti, E., Egner, S., Herbst, T., M., Ragazzoni, R., Reymann, D. and Xu, W. *LINC-NIRVANA: optical design of an interferometric imaging camera SPIE 6269,11* (2006)
- [5] Königl, A. and Pudritz, R., *Protostars and Planets IV*, p.7591 (2000)
- [6] Garcia, P.,J.,V., Ferreira, J., Cabrit, S., and Binette, L., *A&A*, 377, 589 (2001)
- [7] Shang, H., Glassgold, A.E., Shu, F.H. and Lizano, S., *ApJ*, 564, 853 (2002)
- [8] Nisini, B., Bacciotti, F., Giannini, T., Massi F., Eisloffel, J., Podio, L., and Ray, T.P., *A&A*, 441, 159 (2005)
- [9] Reipurth, B., Heathcote, S., Morse J., Hartigan P. and Bally, J., *AJ*, 123, 362 (2002)
- [10] Arcidiacono, C. et al., *Appl.Optics*, 43, 22 (2004)
- [11] Ragazzoni, R., Diolaiti, E., Farinato, J., Fedrigo, E., Marchetti, E., Tordi M. and Kirkman D., *A&A*, 396, 731 (2002)
- [12] Fini, L., Carbillet, M. and Riccardi, A., in *ASP Conf. Ser. ADASS X*, eds F. A. Primini & F. R. Harnden, 253 (2001)
- [13] Correia, S., Carbillet, M., Boccacci, P., Bertero, M., and Fini L., *A&A*, 387, 733 (2002)
- [14] Bertero, M. and Boccacci, P., *A&AS*, 144, 181 (2000)
- [15] Hudson, H., M. and Larkin, R., S., *IEEE Trans. Med. Im.* 13, 601 (1995)
- [16] La Camera, A., Desiderá, G., Arcidiacono, C., Boccacci, P. and Bertero, M., *A&A*, 471, 1091 (2007)
- [17] Anconelli, B., Bertero, M., Boccacci, P., Desiderá, G., Carbillet, M. and Lanteri, H., *A&A*, 460, 349 (2006)
- [18] Peng, C.,Y., Ho, L.,C., Impey, C.,D. and Rix, H.,W, *ApJ*, 124, 266 (2002)